A realistic modeling of fluid infiltration in thin fibrous sheets

Sudhakar Jaganathan,[1] Hooman Vahedi Tafreshi,[2,a)] and Behnam Pourdeyhimi[1]
[1]*Nonwovens Cooperative Research Center, The Nonwovens Institute, NC State University, Raleigh, North Carolina 27695-8301, USA*
[2]*Department of Mechanical Engineering, Virginia Commonwealth University, Richmond, Virginia 23284-3015, USA*

(Received 17 September 2008; accepted 1 May 2009; published online 9 June 2009)

In this paper, a modeling study is presented to simulate the fluid infiltration in fibrous media. The Richards' equation of two-phase flow in porous media is used here to model the fluid absorption in unsaturated/partially saturated fibrous thin sheets. The required consecutive equations, relative permeability, and capillary pressure as functions of medium's saturation are obtained via fiber-level modeling and a long-column experiment, respectively. Our relative permeability calculations are based on solving the Stokes flow equations in partially saturated three-dimensional domains obtained by imaging the sheets' microstructures. The Richards' equation, together with the above consecutive correlations, is solved for fibrous media inclined with different angles. Simulation results are obtained for three different cases of upward, horizontal, and downward infiltrations. We also compared our numerical results with those of our long-column experiment and observed a good agreement. Moreover, we establish empirical coefficients for the semianalytical correlations previously proposed in the literature for the case of horizontal and downward infiltrations in thin fibrous sheets. © *2009 American Institute of Physics*. [DOI: 10.1063/1.3141737]

I. INTRODUCTION

Infiltration is the basic mode of spontaneous fluid transport in most fibrous materials. The word "spontaneous" here is used to refer to the fluid uptake solely due to the capillary pressure. The spontaneous infiltration can be influenced by the gravitational forces depending on the material angle of inclination. Upward fluid infiltration in thin fibrous materials has been studied by many researchers in the last decades (see Refs. 1 and 2 for a complete review). Many authors have used the pioneering model of Washburn[3] to study the fluid infiltration.[4–9] Washburn's approach of modeling complex interstitial pore space with equivalent capillary tubes has been often criticized in the literature.[10–12] To this date, there is no fundamental analytical theory to deduce the equivalent capillary of a porous medium and investigators have to rely on empiricism.[13] The other shortcoming of the Washburn's model is its assumption of fully saturated media below the wetting front. This assumption is known to break down when the flow is influenced by the gravity for instance.[14]

On a parallel track, fluid infiltration problems have also been studied using the so-called Richards' equation[15] originally developed for granular porous media.[16–18] Richards' equation is based on the modification of the Darcy's law for partially saturated media. Unlike the work of Washburn, the pore space is not modeled by series of equivalent capillary tubes in the Richards' model. Further assumptions here are that the capillary pressure is a function of the local fluid content θ (volume of fluid/volume of media), inertial forces are neglected, and the flow is laminar. Based on these assumptions, the Darcy's law for unsaturated flow in the presence of gravitational effects can be written as[19]

$$u = -K(\theta)(\nabla\psi(\theta) + \rho g \sin\alpha), \tag{1}$$

where K, ψ, ρ, and g are the permeability, capillary pressure, fluid density, and gravitational acceleration. Here α is the angle of inclination of the sheet with respect to horizon (see Fig. 1). Also note here that $K=k/\mu$, where k is the intrinsic (or Darcy's) permeability of the medium. When Eq. (1) is combined with the continuity equation, we have

$$\frac{\partial\theta}{\partial t} + \frac{\partial u}{\partial x} = 0. \tag{2}$$

Substituting from Eq. (1), we have

$$\frac{\partial\theta}{\partial t} = \frac{\partial}{\partial x}\left(K(\theta)\frac{\partial\psi}{\partial x}\right) + \rho g \sin\alpha \frac{\partial K(\theta)}{\partial x}. \tag{3}$$

Richards's equation is a highly nonlinear advection-diffusion-type equation, i.e., analytical solution is seldom possible. Richards' equation can be also written in terms of pressure but numerical solution seems to suffer from poor mass conservation.[19] One-dimensional (1D) form of Richards' equation can be also written in terms of saturation (Θ = volume of fluid/volume of pore) as

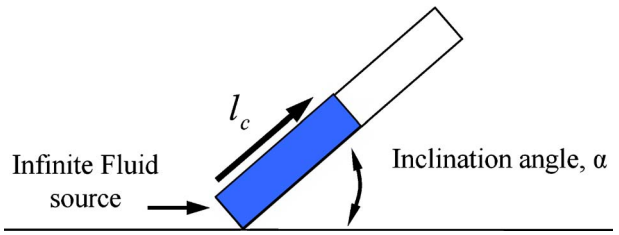

FIG. 1. (Color online) A schematic representation of 1D fluid infiltration problem considered in this paper.

a)Author to whom correspondence should be addressed. Electronic mail: htafreshi@vcu.edu. Tel.: 804-828-9936. FAX: 804-827-7030.

 © 2009 American Institute of Physics

Downloaded 09 Jun 2009 to 128.172.192.39. Redistribution subject to AIP license or copyright; see http://jap.aip.org/jap/copyright.jsp

$$\theta_s \frac{\partial \Theta}{\partial t} = \frac{\partial}{\partial x}\left(D(\Theta)\frac{\partial \Theta}{\partial x}\right) + \rho g \sin \alpha \frac{\partial K(\Theta)}{\partial x}, \quad (4)$$

where $D(\Theta)=K(\Theta)\partial\psi/\partial\Theta$ is the diffusivity coefficient. Here saturation Θ is related to moisture content θ by $\Theta=\theta/\theta_s$, where θ_s is the moisture content at complete saturation, i.e., porosity of the medium. A solution for Eq. (4) exists in terms of error function when diffusivity coefficient is constant and $\alpha=0$.[1] In order to solve the above equation, one needs to have the permeability and capillary pressure in terms of saturation, i.e., $K(\Theta)$ and $\psi(\Theta)$.

In Sec. II, we present our modeling approach to obtain an expression for $K(\Theta)$. This will be followed by a description of our long-column experiment designed to establish a relationship between capillary pressure and saturation $[\psi(\Theta)]$. In Sec. III, we present our finite element solution of Richards' equation for upward, horizontal, and downward fluid infiltrations. In this section we also compare our modeling results with experimental data and the available modeling in the literature. Moreover, we obtain empirical coefficients for the semianalytical correlations that were previously reported in the literature for the case of horizontal and downward infiltrations.

II. CONSTITUTIVE EQUATIONS

A. Relative permeability-saturation relationship

In order to find the relative permeability as a function of saturation $K(\Theta)$, we utilize three-dimensional images of the medium's microstructure. These images are obtained via digital volumetric imaging (DVI) technique. DVI instrument operates based on a block-face fluorescence imaging technique.[20] It continuously sections and images the material embedded in a polymeric resin. The resulting two-dimensional (2D) cross-sectional images are then combined together to construct a 3D image. Resolution of the images ranges from 0.48 to 4.48 μm/pixel with a field of view ranging from 0.45 to 4.4 mm. For more information on processing 3D images and their applications in fluid flow and pore size characterizations, readers are referred to our recent works.[21,22]

For the current study, hydroentangled nonwoven sheets made up of polyester fibers with a fiber length of 3 cm and an average diameter of about 13 μm were produced in the pilot facilities of the Nonwovens Institute at NC State University. These materials had an average porosity of $\theta_s=95\%$. Hydroentangling is one of the most popular methods used for bonding loose fibers in a nonwoven fiber web. The underlying mechanism in hydroentanglement is the exposure of fibers to a nonuniform spatial pressure field created by successive banks of closely packed high-speed waterjets. The impact of waterjets with fibers in a fiber web displaces and rotates them with respect to their neighbors and results in fiber entanglement leading to a coherent and strong fabric.[23,24] The fiber web used for the hydroentangling process here was prepared via carding process. Our hydroentangled fabric was stained using a Nile Red fluorescent dye before the imaging. A resolution of 2.2 μm/voxel was selected for the sectioning imaging. Figure 2 shows a DVI image of our hydroentangled fabric used in this study.

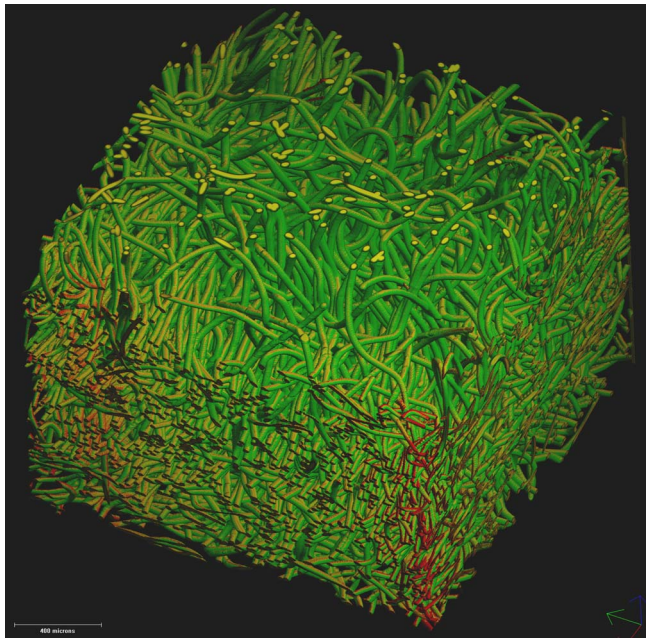

FIG. 2. (Color online) A 3D image of our polyester hydroentangled nonwoven fabric obtained via DVI. Fiber diameter d_f is about 13 μm and the materials' average porosity is $\theta_s=95\%$.

To find the relative permeability as a function of saturation one has to saturate the sample to different levels and predict the permeability of this partially saturated medium. Landeryou *et al.*[19] used an experimental technique wherein fluid was introduced at different flow rates into nonwoven sheets and the relative permeability-saturation relationship was found from the translational speed of the fluid front. These authors obtained a cubic relationship between the relative permeability and saturation of the medium

$$K(\Theta) = K_s \Theta^3. \quad (5)$$

This expression is similar to the general power-law relationship of Brooks and Corey,[25]

$$K(\Theta) = K_s \Theta^{\varepsilon}, \quad (6)$$

where $\varepsilon=4$ is reported to be a typical value for granular porous media.[14] In our work, we use an image analysis technique known as full-morphology method to saturate a virtual 3D model of the material's microstructure to different levels and predict its permeability. The virtual images, as mentioned before, are obtained via DVI imaging. The full-morphology approach is a quasistatic image analysis method described in details in the works of Hazlett[26] and Hilpert and Miller.[27] In the current paper, we use a modified full-morphology algorithm developed based on the works of Hilpert and Miller[27] and implemented in the GEODICT code from Fraunhofer ITWM (www.Geodict.com). Readers are referred to Schulz *et al.*[28] for a detailed description of this implementation. This algorithm assumes that the pore space of the medium is initially fully saturated with a nonwetting phase and is connected from one side to a large reservoir of a wetting fluid. The wetting fluid, then, intrudes into the

Downloaded 09 Jun 2009 to 128.172.192.39. Redistribution subject to AIP license or copyright; see http://jap.aip.org/jap/copyright.jsp

fibrous structure as the reservoir's pressure is increased. Based on the Young–Laplace equation $p_c = 2\sigma \cos\theta / r$, it is assumed that only certain pore diameters can be intruded for each pressure increment. In order to simulate this quasistatic fluid intrusion, a spherical structuring element (B_r) of an increasing radius of r is developed and is used in morphological operation "erosion" defined as

$$\varepsilon_{B_r}(X) = \{x : B_{x,r} \subseteq X\}, \tag{7}$$

where X is the pore space and $B_{x,r}$ is the structuring element centered at point x.[28] The radius r of these structuring elements is obtained using the Young–Laplace equation. The erosion operation results in the center points, where a given sphere can fit without intruding the fiber boundaries. The erosion procedure is then followed by a connectivity analysis which results in the removal of all those eroded pore spaces which are not connected to the reservoir. In order to find the pore volume which has been intruded for a particular pressure, the eroded space is then dilated using the same structuring element defined as

$$D_{B_r}\lfloor \varepsilon_{B_r}(X) \rfloor = \{x : B_{x,r} \cap \varepsilon_{B_r}(X) \neq \emptyset\}. \tag{8}$$

This dilation step gives a particular saturation level of wetting phase fluid. Once this dilation step is completed, pressure is incremented in predetermined steps to find the next smaller structuring element using the Young–Laplace equation, and the above procedure is repeated to get find the next saturation level. Note that the wetting fluid reservoir can be placed at any side of the simulation domain. Here all other boundaries are assumed to be impermeable to the fluid. Note also that the numeric value used for the contact angle is not important in this analysis as the objective is finding the relation between the relative permeability and saturation (not the capillary pressure).

As the image shown in Fig. 2 is too large to fit our available computational memory, we crop the image to a size of $400 \times 400 \times 400$ voxels. This size is believed to be large enough to represent the whole medium. For more discussion on the importance of the domain size readers are referred to our previous work.[21] In Fig. 3, we show fibrous structure which has been saturated to different levels by full-morphology method.

At each increment of wetting fluid intrusion (each level of saturation), one can find the medium's permeability by solving the Stokes flow equation with periodic boundary conditions inside the microstructure. The Stokes equations for conservation of mass and momentum are as follows:

$$\frac{\partial v_x}{\partial x} + \frac{\partial v_y}{\partial y} + \frac{\partial v_z}{\partial z} = 0, \tag{9}$$

$$\frac{\partial p}{\partial x} = \mu\left(\frac{\partial^2 v_x}{\partial x^2} + \frac{\partial^2 v_x}{\partial y^2} + \frac{\partial^2 v_x}{\partial z^2}\right), \tag{10}$$

$$\frac{\partial p}{\partial y} = \mu\left(\frac{\partial^2 v_y}{\partial x^2} + \frac{\partial^2 v_y}{\partial y^2} + \frac{\partial^2 v_y}{\partial z^2}\right), \tag{11}$$

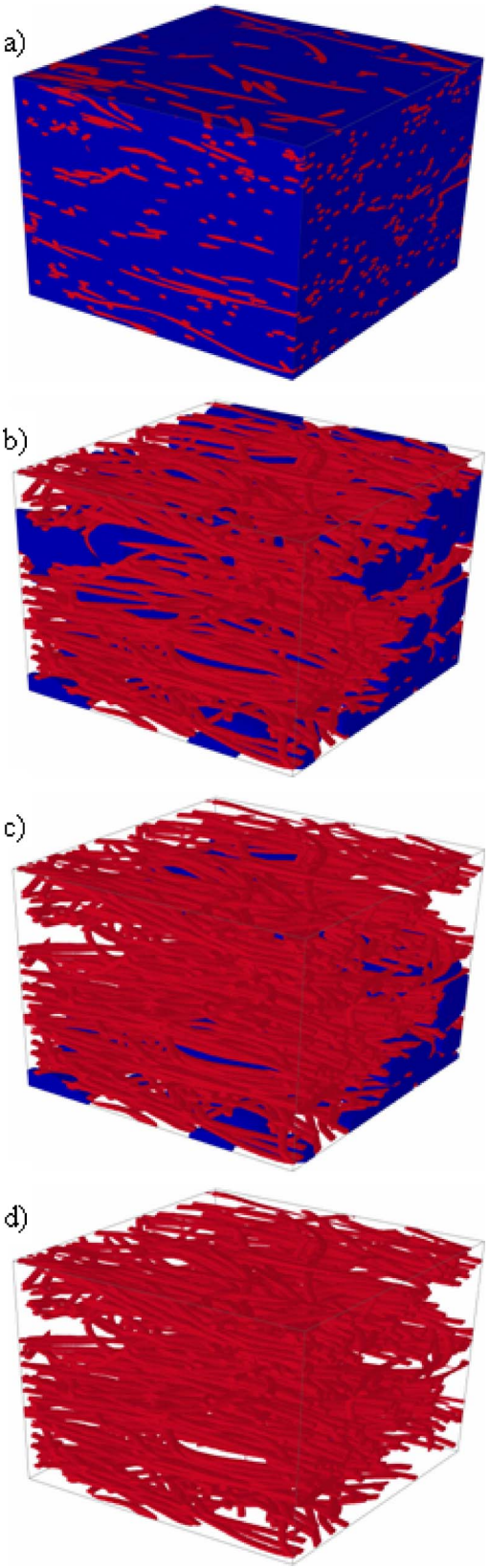

FIG. 3. (Color online) A $708 \times 708 \times 708$ μm^3 subdomain of the image shown in Fig. 2 is considered here for full-morphology simulation. Wetting fluid saturation: (a) 0%, (b) about 50%, (c) about 75%, and (d) 100%.

$$\frac{\partial p}{\partial z} = \mu\left(\frac{\partial^2 v_z}{\partial x^2} + \frac{\partial^2 v_z}{\partial y^2} + \frac{\partial^2 v_z}{\partial z^2}\right), \tag{12}$$

where ν_x, ν_y, and ν_z are velocity in the x, y, and z directions,

Downloaded 09 Jun 2009 to 128.172.192.39. Redistribution subject to AIP license or copyright; see http://jap.aip.org/jap/copyright.jsp

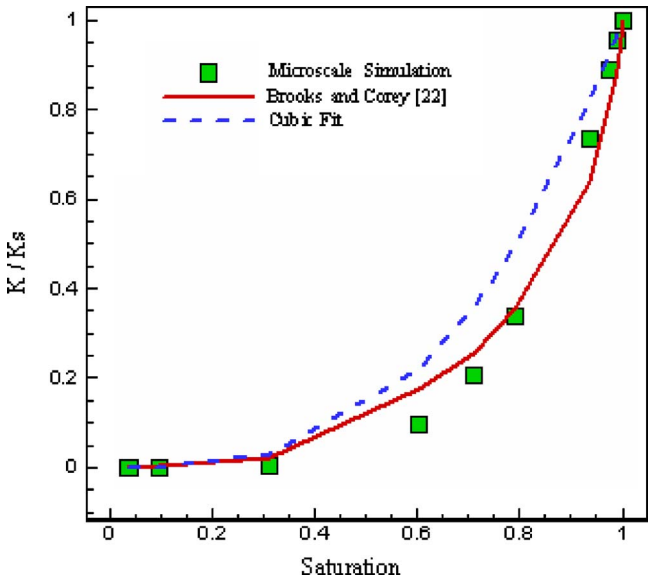

FIG. 4. (Color online) Relative permeability-saturation relationship obtained via full-morphology method and shown in a dimensionless form (K/K_s).

respectively. GEODICT treats each voxel as a computational cell and circumvent the mesh generation process in the complex 3D geometry of a fibrous medium. Based on Darcy's law the relations between mean velocity and pressure drop in each direction are as follows:

$$v_x = \frac{1}{\mu}\left(k_{xx}\frac{\partial p}{\partial x} + k_{xy}\frac{\partial p}{\partial y} + k_{xz}\frac{\partial p}{\partial z}\right), \tag{13}$$

$$v_y = \frac{1}{\mu}\left(k_{yx}\frac{\partial p}{\partial x} + k_{yy}\frac{\partial p}{\partial y} + k_{yz}\frac{\partial p}{\partial z}\right), \tag{14}$$

$$v_z = \frac{1}{\mu}\left(k_{zx}\frac{\partial p}{\partial x} + k_{zy}\frac{\partial p}{\partial y} + k_{zz}\frac{\partial p}{\partial z}\right), \tag{15}$$

where $k_{ij}(i,j=x,y,z)$ is the intrinsic permeability tensor. Here we use a finite difference scheme of GEODICT code.[29] Note that during these simulations, the nonwetting phase is considered as immobile obstructions to the fluid flow (i.e., the nonwetting phase is considered as a solid phase) which increases the resistance to the fluid flow. This also implies that there is no momentum transfer between phases. For more information on these simulations readers are referred to our previous publication.[30] Note that k_{xz} and k_{yz} are almost three orders of magnitude smaller than k_{zz}. We, therefore, neglect any fluid flow in the x and y directions (inplane flow) in formulating our model. As mentioned earlier in the introduction, the intrinsic permeability can be converted to permeability of the medium by $K=k/\mu$.

When the nonwetting phase is completely removed we obtain saturated permeability K_s. The absolute (fully saturated) permeability was found to be $K_s=0.01$ mm^3 s/g. We fitted the equation of Brooks and Corey[25] (Eq. (6)) and the cubic relation of Landeryou *et al.*[19] (Eq. (5)) to our data. The equation of Brooks and Corey[25] with $\varepsilon=4.6$ resulted in a much better fit, as can be seen in Fig. 4. This deviation from the cubic relation might be due to the difference between the

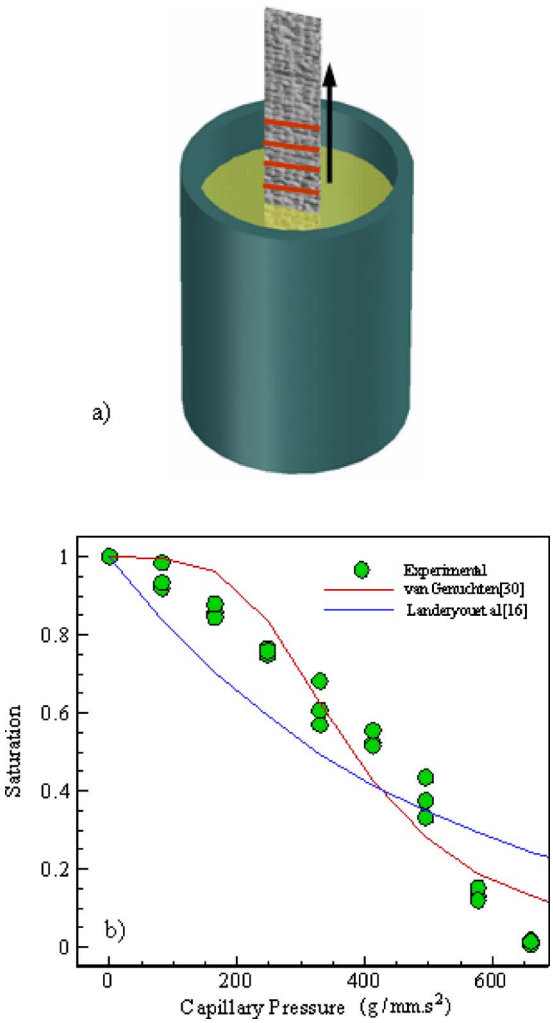

FIG. 5. (Color online) (a) A schematic of the long-column test. (b) Our experimental results are shown along with the correlations of van Genuchten (Ref. 33) and Landeryou *et al.* (Ref. 19) fitted to our data.

microstructure of the nonwoven material (hydroentangled fabric) used in our work and that of Landeryou *et al.*[19] (needle-punched fabric). Also note here that relative permeability (K/K_s) tends to zero when saturation is smaller than 0.4, suggesting that there is a percolation threshold for the fluid infiltration. Neither of the cubic or power-law relationships can capture this feature.

B. Capillary pressure-saturation relationship: Experiment

Landeryou *et al.*[19] used an autoporosimeter[31] to obtain a relationship between the capillary pressure and saturation. The work of Landeryou *et al.*[19] was conducted in the material's thickness and, therefore, cannot be used here to study the inplane infiltration. Note that most nonwoven materials have anisotropic layered microstructures, i.e., measurements made in the thickness direction cannot be used in other directions. We, therefore, used a long-column method[14,32] to obtain a relationship between the capillary pressure and saturation. In this method, a long strip of the fibrous sheet was cut and hung in an infinite source of wetting fluid [as shown schematically in Fig. 5(a)] until an equilibrium height was

Downloaded 09 Jun 2009 to 128.172.192.39. Redistribution subject to AIP license or copyright; see http://jap.aip.org/jap/copyright.jsp

reached after about 24 h. The samples were then cut into equal segments and the saturation of each segment was found by measuring their wet and dry weights with an analytical microbalance having a resolution of 1 μg. Saturation of the sample is obtained by

$$\Theta = \frac{M_w - M_d}{\rho_f v_b - M_d/\gamma}, \tag{16}$$

where M_w and M_d are the wet and dry weights of the segments and ρ_f and v_b are the fiber density (1.39×10^{-3} g/mm^3) and bulk volume of the material. Here γ is the relative density given by ρ_f/ρ_{flu}, where $\rho_{\text{flu}}=8.41 \times 10^{-4}$ g/mm^3 is the fluid density (mineral oil from Sigma-Aldrich with a viscosity of 0.03 Pa s). To suppress any fluid redistribution, we froze the samples before cutting using a dry ice. Capillary pressure is given by $\psi=\rho g h$, where h is height of each segment from datum line. The above test was repeated three times and the results are shown in Fig. 5(b).

It is also possible to develop a capillary pressure-saturation relationship by conducting a quasisteady microscale modeling similar to that of Schulz *et al.*[28] Such a modeling, however, requires an accurate estimation of the contact angle between the fluid and the fibrous media which is not easy to determine. With the above experiments we could circumvent this problem.

In Fig. 5(b), we fitted the empirical correlation of van Genuchten[33] to our experimental data,

$$\Theta = [1 + (\psi/\psi^*)^n]^{-m}, \tag{17}$$

where ψ^*, m, n are empirical constants. Further approximation[33] $m=1-1/n$ was also considered to simplify the equation. It is worth mentioning that the van Genuchten's model has also been used by Iryo and Rowe[34] to study fluid infiltration in nonwovens used in geotextile applications. The empirical fit of van Genuchten correlation to our experimental data results in $\psi^*=342$ g/mm s^2 and $n=4$. We also fitted the exponential relation $\Theta=\exp(\psi/\psi^*)$ of Landeryou *et al.*[19] but did not observe a good match, as can be seen in Fig. 5(b).

III. NUMERICAL SIMULATIONS

Having the constitutive equations obtained from Sec. II we can now numerically solve the Richards' equation to simulate the fluid absorption in our fibrous sheets. FLEXPDE program was used here to solve the Richards' equation along with the aforementioned relative permeability-saturation and capillary pressure-saturation relationships,

$$\theta_s \frac{\partial \Theta}{\partial t} = \frac{\partial}{\partial x}\left(D(\Theta) \frac{\partial \Theta}{\partial x} \right) + \rho g \sin \alpha \frac{\partial K(\Theta)}{\partial x}, \tag{18}$$

$$K(\Theta) = K_s \Theta^{4.6}, \tag{19}$$

$$\frac{d\psi}{d\Theta} = -\frac{\psi^* \Theta^{-n/(n-1)}}{(n-1)[1-\Theta^{n/(n-1)}]^{(n-1)/n}}. \tag{20}$$

FLEXPDE is a general purpose mathematical program developed by PDE Solutions, Inc. for solving partial differential equations using finite element method. The above equations are coded in FLEXPDE and are solved in a 1D domain with the following boundary and initial conditions: $\Theta(x=0,t)=1$, $\Theta(x=l,t)=0$, and $\Theta(x,0)=0$, where l is the length of the domain. To ensure that the results of our finite element simulations are not mesh dependent, we considered different numbers of element counts in our trial simulations. The results presented here are obtained with 60 elements and are believed to be mesh independent.

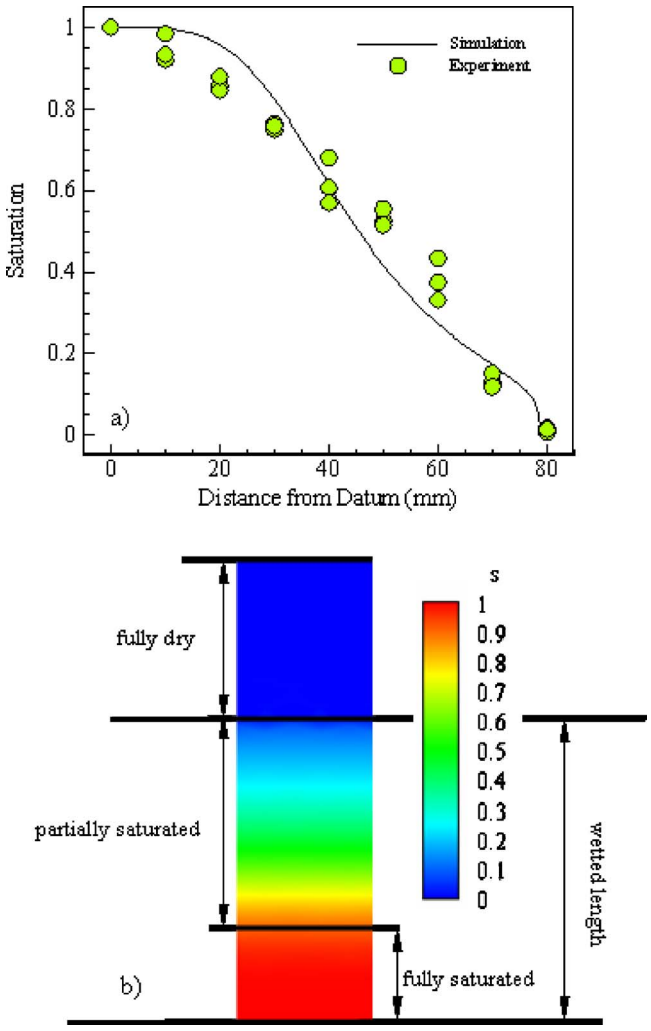

FIG. 6. (Color online) (a) Saturation profiles after $t=86\,400$ s for upward infiltration obtained from simulation and experiment. (b) A contour plot of the medium's saturation obtained from our simulation at $t=86\,400$ s. Note that the1D results are presented in a 2D domain for better visualization.

A. Upward infiltration

The results of the upward infiltration are shown in Fig. 6(a) where a comparison is made between the saturation profile obtained from our simulations and experiment for $\alpha=90°$ at $t=86\,400$ s. A good agreement between our simulations and experiments is evident. It can also be seen that there is a steep saturation gradient under the wetting front. This can be observed also in the contour plot of Fig. 6(b) (1D simulation results are copied in the y-direction to produce a 2D contour plot for better visualization). As mentioned before, Washburn's equation cannot predict this partially saturated region.

Downloaded 09 Jun 2009 to 128.172.192.39. Redistribution subject to AIP license or copyright; see http://jap.aip.org/jap/copyright.jsp

In order to check the accuracy of our simulations, an experimental setup was build to allow capturing the images of fluid infiltration. A Computar® dynamic video camera was used to capture images at a rate of 1 frame per second. Imaging the entire length of the fluid rise requires a camera with a high resolution, and simultaneously, a large field of view. Our camera had a field of view of about 20 mm and so we limited our imaging to the first 50 s of the fluid infiltration experiment.

Once the images were captured [see Fig. 7(a)], they were processed to extract the wetting front so that the rate of infiltration could be calculated. The images were first subjected to a gray-level relaxation process (see Pratt[35] for more details) to improve the contrast between the fluid and material [see Fig. 7(b)]. A median filter was then used to remove any noisy pixels from the image. This was followed by a single thresholding step to convert gray scale images to binary images, as shown in Fig. 7(c). This final step provided us with the wetted front. Note that the wetted front is not distinguishable with naked eyes. To eliminate the operator's error, the wetted heights were considered to be the height where the first white pixel was encountered when moving down from the top of the image, as shown in Fig. 7(c). In principle, one can measure an average saturation level across the width of eth sample, e.g., 20%, and compare it with the height corresponding to that saturation (e.g., 20%) obtained from the simulation. We decided to go ahead with the minimum saturation (maximum height) and compared it with the height corresponding to the zero-saturation height from the simulations. This is because it was easier to measure the height associated with the minimum saturation rather than 20%, for instance, as it required accurate saturation measurements.

Our wetted length data (three separate experiments) are plotted versus time in Fig. 8(a) along with the predictions of our numerical simulation. It can be seen that there is a good agreement between the experiment and the model. The average equilibrium height (maximum height) that fluid could reach was about 80 mm and it is in good agreement with our numerical results being 80.4 mm (not shown in the figures).

In Fig. 8(b), we show a comparison between the saturation profiles and the wetted lengths for various angles of inclination ($\alpha > 0°$) at $t=1000$ s obtained from numerical simulations. It can be seen that increasing the inclination angle slows the fluid infiltration.

B. Horizontal infiltration

For the case of horizontal infiltration in the absence of inertial effects, a simple analytical equation can be derived for the wetted length (l_w) according to the Poiseuille's equation for flow through a capillary tube[3]

$$l_w = C\sqrt{t}, \tag{21}$$

where $C=\sqrt{r_c\sigma \cos \theta/2\mu}$. Here r_c is the equivalent capillary radius and σ, θ, and μ are surface tension, wetting angle, and viscosity of the fluid. In terms of saturated permeability K_s, the constant C can be written as $C=\sqrt{2K_s\psi^*}$, where ψ^* is known as the capillary potential of the medium and should be obtained empirically (Eames *et al.*[11]). In spite of its underlying oversimplified assumptions, Washburn's equation forms a good framework for analyzing the horizontal infiltration due to its simplicity.

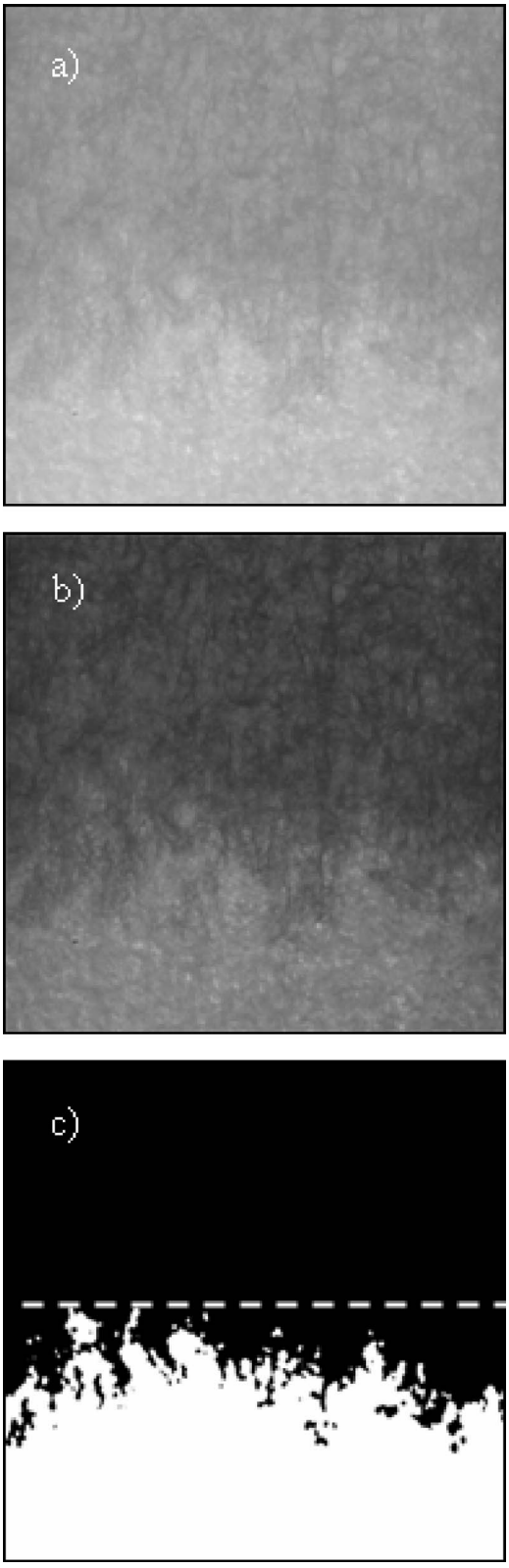

FIG. 7. The image processing steps used for determining the wetting front: (a) initial gray scale image, (b) the image after the gray level relaxation, and (c) the image after the thresholding.

In the case of horizontal infiltration $\alpha=0°$, Richards' equation (Eq. (18)) reduces to

Downloaded 09 Jun 2009 to 128.172.192.39. Redistribution subject to AIP license or copyright; see http://jap.aip.org/jap/copyright.jsp

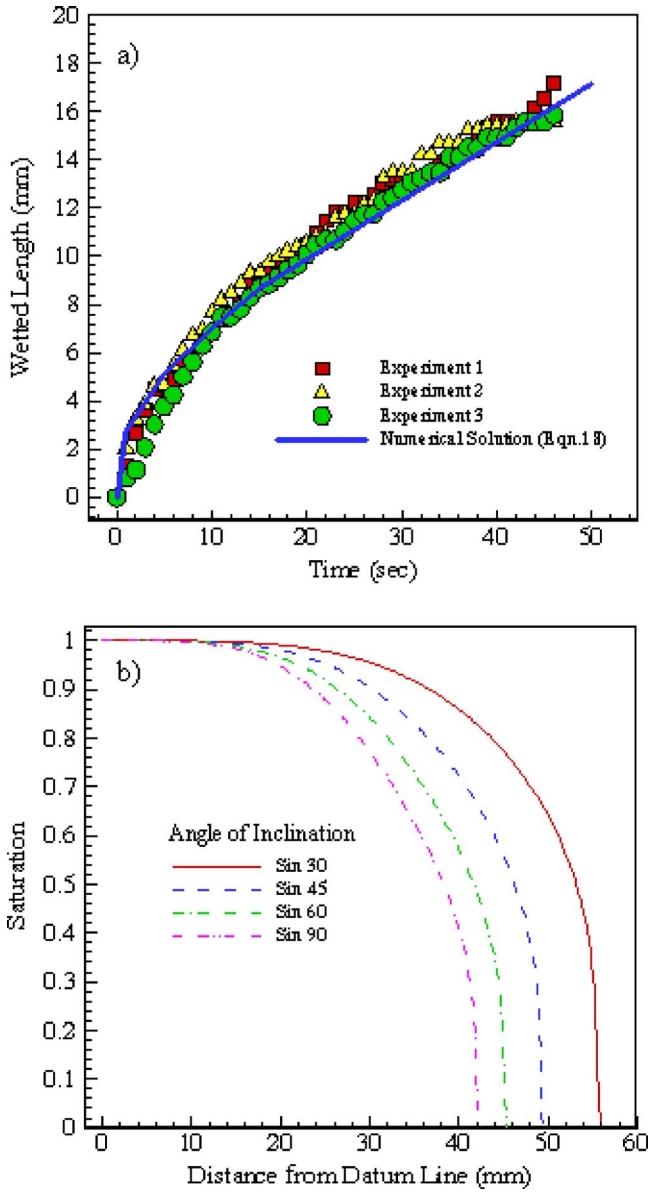

FIG. 8. (Color online) Numerical solution of Richards' equation: (a) wetted length vs time for $\alpha=90°$ and (b) saturation profile at $t=1000$ s for various inclination angles.

$$\frac{\partial\Theta}{\partial t}=\frac{\partial}{\partial x}\left(\frac{D(\Theta)}{\theta_s}\frac{\partial\Theta}{\partial x}\right). \tag{22}$$

A well known solution to the above equation for the rate of infiltration in terms of Boltzmann transformation[14,19,36,37] is

$$l_c^2=\varphi t, \tag{23}$$

where φ is an empirical constant. It is worth mentioning that the above equation implies that the wetted length is proportional to $\sqrt{t}$ as was originally proposed by Washburn. Landeryou *et al.*[19] assumed $\varphi=\lambda\sqrt{2K_s\psi^*/\theta_s}$, where λ is an empirical constant to be obtained from curve fitting the numerical solution of Eq. (22).

Figure 9 shows the wetted length versus $\sqrt{t}$ obtained by solving Eq. (22) using the FLEXPDE software. Note the linear relationship between the wetted length and $\sqrt{t}$. The solution of Eq. (22) is fitted into these results to obtain $\lambda=0.89$. This

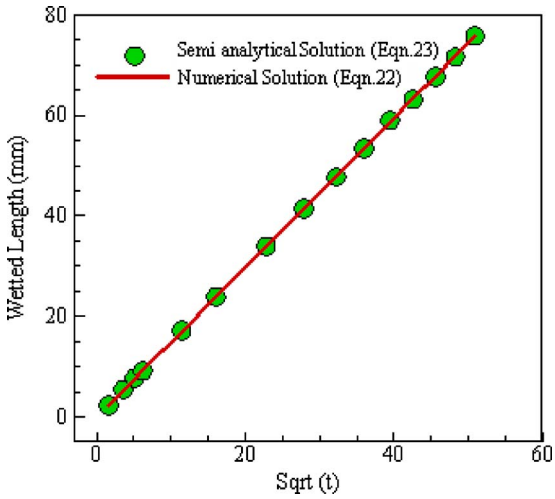

FIG. 9. (Color online) Numerical solution of Richards' equation for $\alpha=0°$: wetted length vs $\sqrt{t}$. Equation (23) is fitted to the numerical solution to yield $\varphi=0.89$.

indicates that the wetted length increases slower than what the Washburn's equation predicts. This effect can be attributed to the fact that the fluid front is not fully saturated as Washburn model assumes and so reduces the relative permeability of the medium. It is worth noting that Landeryou *et al.*[19] obtained a coefficient of $\varphi=0.77$ for their needle-punched fibrous media.

C. Downward infiltration

For the case of downward inclination $\alpha<0$, Richards' equation has a solution for the wetted length as a function of time obtained by Philip[38] in the form of a power series,

$$l_c=\xi\sqrt{t}+\varsigma t+\omega t^{-3/2}+\cdots+f_m(\Theta)t^{m/2}+\cdots, \tag{24}$$

where the coefficients are functions of Θ.[14] For all practical purposes, we only need the first two terms of this power series,[38]

$$l_c=\xi\sqrt{t}+\varsigma t. \tag{25}$$

According to this equation, at the initial stages of infiltration, the first term in Eq. (25) is the dominant term.[14] Therefore, in analogy with the case of horizontal infiltration, we assume $\xi=\lambda\sqrt{2K_S\psi^*/\theta_s}$. At longer times, however, infiltration becomes proportional to t as the gravitational forces overtake the capillary forces. Here we substitute $\varsigma=\chi(K_s\rho g\sin\alpha/\theta_s)$ as proposed by Landeryou *et al.*[19]

Same as the case of horizontal infiltration, we use our numerical simulations (Eq. (18)) to obtain the required empirical coefficients (λ and χ). Figure 10 shows the numerical solution of Richards' equation (Eq. (5)). Fitting Eq. (18) to these results, we obtain $\lambda=0.89$ and $\chi=0.69$.

IV. CONCLUSIONS

Fluid infiltration problems involving fibrous materials have long been studied using Washburn's model. While Washburn's equation is a good approximation for the fluid infiltration, it has two major shortcomings. It models the complex pore spaces of a fibrous medium by a series of

Downloaded 09 Jun 2009 to 128.172.192.39. Redistribution subject to AIP license or copyright; see http://jap.aip.org/jap/copyright.jsp

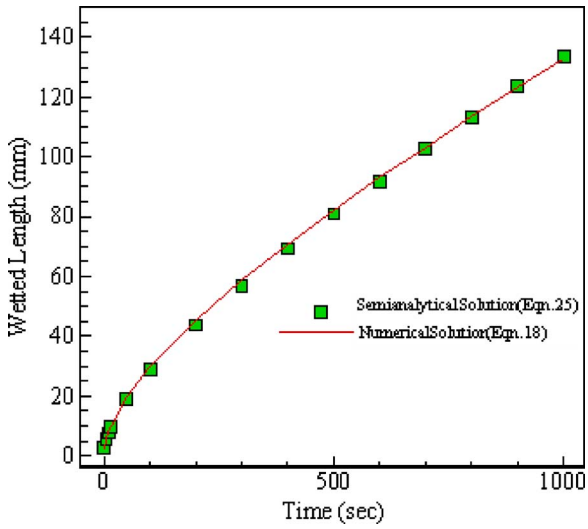

FIG. 10. (Color online) Numerical solution of Richards' equation for $\alpha < 0°$: wetted length vs $\sqrt{t}$. Equation (25) is fitted to the numerical solution to yield $\varphi=0.89$, $\xi=0.69$.

unidirectional discrete capillary tubes and so requires an equivalent capillary diameter. Furthermore, Washburn's model assumes a complete saturation under the wetting front which is obviously inaccurate.

In this paper, we have used a more complete model based on the work of Richards[15] to numerically simulate the fluid infiltration into inclined fibrous sheets. Here, for the first time, we have combined the Richards' equations with the results of 3D microscale relative permeability computations in fibrous microstructures obtained from imaging. In particular, it is shown that the relative permeability-saturation relationship for a fibrous thin sheet has a form similar to that proposed by Brooks and Corey[25] with an exponent of $\varepsilon=4.6$. Our capillary-saturation relationship was obtained experimentally and was observed to obey the model of van Genuchten.[33]

Fluid infiltration simulations are conducted for three different configurations of upward, horizontal, and downward infiltrations. To validate our simulations, we compared our numerical results with those of our long-column test and observed a good agreement. The rate of fluid height rise was obtained via imaging and was found to be in good agreement with our numerical simulations. Furthermore, we obtained empirical coefficients for the correlations proposed by Landeryou *et al.*[19] and Philip[38] for horizontal and downward infiltrations in thin fibrous sheets, respectively. The rate of fluid infiltration was shown to be similar to that predicted by the Washburn's model but with a slower rate.

ACKNOWLEDGMENTS

The current work is supported by the Nonwovens Cooperative Research Center. Their support is gratefully acknowledged. We would like to thank Dr. Shim of The Nonwovens Institute for her help in setting up the experiments.

[1] *Absorbent Technology*, Textile Science and Technology Vol. 13, edited by P. K. Chatterjee and B. S. Gupta (Elsevier, New York, 2002).
[2] N. Pan and W. Zhong, Textile Progress **38**, 1 (2006).
[3] E. W. Washburn, Phys. Rev. **17**, 273 (1921).
[4] T. Gillespie, J. Colloid Sci. **14**, 123 (1959).
[5] A. Marmur and R. D. Cohen, J. Colloid Interface Sci. **189**, 299 (1997).
[6] A. Hamraoui and T. Nylander, J. Colloid Interface Sci. **250**, 415 (2002).
[7] L. Zhu, A. Perwuelz, M. Lewandowski, and C. Campagne, J. Adhes. Sci. Technol. **22**, 745 (2008).
[8] J. Hyväluoma, P. Raiskinmäki, A. Jäsberg, A. Koponen, M. Kataja, and J. Timonen, Phys. Rev. E **73**, 036705 (2006).
[9] M. Gombia, V. Bortolotti, R. J. S. Brown, M. Camaiti, and P. Fantazzini, J. Appl. Phys. **103**, 094913 (2008).
[10] J. R. Philip, Annu. Rev. Fluid Mech. **2**, 177 (1970).
[11] I. Eames, I. Small, A. Frampton, and A. M. Cottenden, Proc. Inst. Mech. Eng., Part H: J. Eng. Med. **217**, 263 (2003).
[12] N. Mao and S. J. Russell, J. Appl. Phys. **94**, 4135 (2003).
[13] B. J. Mullins, R. D. Braddock, and G. Kasper, Chem. Eng. Sci. **62**, 6191 (2007).
[14] A. T. Corey, *Mechanics of Immiscible Fluids in Porous Media* (Water Resource Publication, Colorado, USA, 1994).
[15] L. A. Richards, Physics (N.Y.) **1**, 318 (1931).
[16] J. R. Philip, Trans. Faraday Soc. **51**, 885 (1955).
[17] W. R. Gardner, Soil Sci. **85**, 228 (1958).
[18] J. Y. Parlange, Soil Sci. **111**, 134 (1971).
[19] M. Landeryou, I. Eames, and A. Cottenden, J. Fluid Mech. **529**, 173 (2005).
[20] D. Chinn, P. Ostendorp, M. Haugh, R. Kershmann, T. Kurfess, A. Claudet, and T. Tucker, ASME J. Manuf. Sci. Eng. **126**, 813 (2004).
[21] S. Jaganathan, H. Vahedi Tafreshi, and B. Pourdeyhimi, Chem. Eng. Sci. **63**, 244 (2008).
[22] S. Jaganathan, H. Vahedi Tafreshi, and B. Pourdeyhimi, J. Colloid Interface Sci. **326**, 166 (2008).
[23] A. Begenir, H. Vahedi Tafreshi, and B. Pourdeyhimi, Text. Res. J. **74**, 178 (2004).
[24] H. Vahedi Tafreshi and B. Pourdeyhimi, Text. Res. J. **74**, 359 (2004).
[25] R. H. Brooks and A. T. Corey, Hydrology Paper No. 3, Colorado State University, 1964.
[26] R. D. Hazlett, Transp. Porous Media **20**, 21 (1995).
[27] M. Hilpert and C. T. Miller, Adv. Water Resour. **24**, 243 (2001).
[28] V. P. Schulz, J. Becker, A. Wiegmann, P. P. Mukherjee, and C. Y. Wang, J. Electrochem. Soc. **154**, B419 (2007).
[29] A. Wiegmann, "Computation of the Permeability of Porous Materials from Their Microstructure by FFF-Stokes," Fraunhofer ITWM Report No. 129, 2007.
[30] S. Jaganathan, H. Vahedi Tafreshi, and B. Pourdeyhimi, Sep. Sci. Technol. **43**, 1901 (2008).
[31] B. Miller and I. J. Tyomkin, J. Colloid Interface Sci. **162**, 163 (1994).
[32] R. E. Collins, *Flow of Fluid Through Porous Materials* (Reinhold, New York, 1961).
[33] M. Th. van Genuchten, Soil Sci. Soc. Am. J. **44**, 892 (1980).
[34] T. Iryo and R. K. Rowe, Geotext. Geomembr. **21**, 381 (2003).
[35] W. K. Pratt, *Digital Image Processing* (Wiley-Interscience Publication, New York, 2001).
[36] L. Boltzmann, Ann. Phys. **289**, 959 (1894).
[37] A. L. Ruoff, D. L. Prince, J. C. Giddings, and G. H. Stewart, Kolloid-Z. **166**, 144 (1959).
[38] J. R. Philip, Soil Sci. **83**, 345 (1957).

Downloaded 09 Jun 2009 to 128.172.192.39. Redistribution subject to AIP license or copyright; see http://jap.aip.org/jap/copyright.jsp